International Forum on Aeroelasticity and Structural Dynamics
IFASD 2024
17-21 June 2024, The Hague, The Netherlands

AUTOMATED TUNING OF A BASELINE FLIGHT CONTROL SYSTEM WITH MANEUVER LOAD ALLEVIATION FOR AN ENERGY-EFFICIENT PASSENGER AIRPLANE

Till Strothteicher[1] **and Nicolas Fezans**[1]

[1]DLR Institute of Flight Systems
Lilienthalplatz 7, 38108 Braunschweig, Germany
till.strothteicher@dlr.de
nicolas.fezans@dlr.de

Keywords: flight control, aeroelastic control, load alleviation

Abstract: This work presents a longitudinal baseline n_z flight augmentation system (FAS) which is representative of those employed in modern fly-by-wire civil aircraft (regarding the pull-up maneuver loads) along with a maneuver load alleviation (MLA) system which reduces sizing loads. These active control functions are applied to a flexible and energy-efficient aircraft. During the iterative aeroelastic optimization of the preliminary aircraft design, the evolution of the aircraft design and structure call for an adjustment of the control system tuning. An optimization-based procedure is proposed to fully automate the multi-objective control tuning process. This brings the aircraft design closer to an automated multidisciplinary optimization loop regarding the active control functions. The proposed design control approach is demonstrated on a mid-range aircraft configuration and the analysis of the closed-loop behavior and maneuver load figures shows a good tracking of the pilot input and a maneuver load alleviation performance of 7.7–10.9% (analyzed for each considered flight point / model separately).

1 INTRODUCTION AND MOTIVATION

The aeroelastic design process of modern aircraft concepts involves sizing the aircraft based on ultimate or design loads, which are partly defined based on the limit loads for specific load cases (e.g., gust, turbulence, and maneuver loads) and a safety factor (typically 1.5, but potentially less, cf. for instance [1, Appendix K]). Alleviation of the gust and maneuver loads offers potential for lightweight construction and/or improved aerodynamic efficiency via higher aspect-ratio wings. The Sustainable and Energy-Efficient Aviation (SE^{2}A) Cluster of Excellence[1] investigates numerous technologies for sustainable and eco-friendly air transport systems. Among the cluster's research activities are concepts for load reduction in conjunction with tools for the (pre-)design of aircraft.

Usually, for the inboard (and heaviest) portion of the wing, sizing loads are defined by the gust and maneuver loads [2]. Without specific control functions, the maneuver loads tend to dominate the other loads, but it is fairly easy to reduce them by deflecting wing surfaces (ailerons, spoilers) upward to shift the lift distribution inboard when the load factor in the fuselage exceeds a certain threshold. Therefore, the maneuver loads can readily be reduced below the peak load levels reached during gust encounters in open loop. Numerous studies have investigated the potential for mass savings through the use of active maneuver load alleviation control in the

[1]`https://www.tu-braunschweig.de/en/se2a`

last fifty years. Early works by White [3], Allison et al. [2], and Johnson et al. [4] have shown this potential as well as the trade-off between reducing the structural weight and improving the aerodynamic efficiency of the aircraft by increasing the wing span.

In comparison, gust loads are much more challenging to alleviate as the sizing gusts are usually of very large amplitude and the control surface have limited authority and deflection rates. With the use of lidar sensors which can detect gusts/turbulence slightly ahead of the aircraft (typically the usable wind information is available about 0.5 s before it effectively reaches the nose of the airplane), significant reductions in peak gust load envelope would be achievable. Direct-detection Doppler lidar sensors for gust load alleivation (GLA) are not very mature yet (TRL 3–4) but could become available in the next 5–10 years. Reductions on the order of 15–20 % of the maximum values can be reached while remaining strictly within the position and rate limits of the control surface actuators [5], compared to about 5–7 % without lidar sensors and with aggressive and much less robust controllers. Methods for designing active gust load alleviation (GLA) controllers with and without lidar sensors have been designed and applied to the considered aircraft configuration (cf. section 3) by the authors' research group, cf. for instance [6], as well as other research groups, e.g., [7]. This paper presents methods to design both a flight augmentation system (FAS) and a maneuver load alleviation (MLA) function to complement the already available GLA controllers. Their design is automated as much as possible so that they can eventually be incorporated into the multidisciplinary optimization of the aircraft.

Integrating load alleviation functions at the aircraft pre-design stage has already been proposed by several groups, e.g. [8–12], and will probably become standard in the next decade. With each iteration of the aircraft design loop, properties affecting the aeroelastic and flight dynamic behavior of the aircraft are changed, which also calls for an update of the various active control functions. In turn, these adapted control functions impact the gust and maneuver load envelopes of the aircraft for which the aircraft structure is sized. To be able to run design loops efficiently and to consider the active control functions while optimizing the aircraft, the control synthesis for the different modes must be automated. The fine tuning of these control functions usually involves fairly complex and time-consuming trade-offs, which can hardly be reproduced in such automated schemes. The intention is therefore not to design the final controllers. Rather, controllers are tuned whose performance is representative of modern longitudinal flight control laws (and not overly optimistic) with respect to the loads. This guides the multidisciplinary optimization into an appropriate region of the design space and ensures that the assumed load reduction performance remains achievable.

The remaining sections are structured as follows: Section 2 provides an overview of relevant prior work on both the design and tuning of control laws based on the vertical load factor n_z and on maneuver load alleviation functions. After introducing the considered aircraft in Section 3, the proposed control design methods are presented in Section 4. Results obtained with the tuned controllers are discussed in Section 5. Finally, Section 6 summarizes this work and provides an outlook.

2 RELEVANT PRIOR WORK

2.1 Baseline Control Law

Given the widespread adoption of n_z-based control laws, there are surprisingly few references on the tuning of such laws. The Airbus A320 normal law is documented in [13]. Regarding automated tuning, nonlinear dynamic inversion (NDI) laws are often considered as a means to force the aircraft to behave like a specific reference model. However, these approaches can lead

to an aggressive controller with very fast closed loop poles or with large actuation levels to force the aircraft to match the reference model's behavior. NDI can however be a solution, if used properly, and can also provide significant added value when the aircraft exhibit a nonlinear behavior, as shown in [14, 15]. Overall, the three references from Airbus [13, 14, 16], published over a period of 19 years, exhibit the same control law structure. The more recent publication, however, delves deeper into the adaption of the parameters with changes to the flight point and the flight phase as well as the compensation of nonlinear effects.

The existing literature on non-automated tuning of load factor-based control laws is also limited, both regarding the structure of the law and its tuning. Much of the research work focuses on the handling qualities of the longitudinal motion, assuming a bare and rigid aircraft with no significant flight augmentation control system (stability augmentation at most, but no command augmentation). Two examples of in-depth investigation of active control system and their impact on the aircraft longitudinal dynamics and the resulting handling qualities can be found in [17, 18]. Without flight augmentation controllers, the poles and zeros of the transfer function from the elevator deflection to the load factor n_z determine both the dynamic response to pilot inputs and the disturbance rejection properties. For such non-augmented aircraft, the link between stick input response and disturbance rejection capabilities led to the definition of handling criteria based on the short-period pole location. The lower bound on the frequency (typically $2\,rad/s$) can be interpreted as a minimum disturbance rejection bandwidth. The upper-bound on the frequency (typically 2.4–2.6 rad/s) prevents excessively forward center-of-gravity locations which would cause a deficit in the maneuverability of the aircraft ($C_{m,\alpha}$ too strongly negative). A minimum damping ratio (typically 0.5–0.7) is specified to prevent having a large resonance at the short-period mode frequency. Using pole placement techniques would make a lot of sense when tuning a few controller gains which do not change the open-loop behavior too drastically. Reference [14] mentions explicitly that a pole placement approach is used to tune the feedback gain, but also mentions with no details that further filters are required to cope with flexible modes (comfort, no coupling with flutter).

Flight augmentation controllers may, as is already the case with an n_z-law, yield a decoupling between disturbance rejection properties and response to stick inputs. As already mentioned, they can include filters and significantly increase the order of the closed-loop dynamic system. One consequence of that is that the simple notion of having a short-period pair of poles that fully define the longitudinal handling qualities can be invalidated. The fact that the link between the pole-zero map and the handling qualities cannot be readily established does not prevent, however, the disturbance rejection and reference (i.e., stick input) tracking properties from being tuned so that good handling qualities are obtained. By adding and tuning a feedforward filter to the pilot command input, the aircraft response can be tuned independently from the feedback gains and disturbance rejection characteristics of the system [14, section 4].

In the following, a similar baseline control law structure and requirements are considered, however the tuning will be performed and automated utilizing frequency-based methods. Such methods were also applied to a baseline controller in [19].

2.2 Maneuver Load Alleviation Function

The references [8–12], mentioned earlier for their investigation of the load alleviation and mass saving potentials, propose a series of maneuver load alleviation (MLA) configurations. For the design of MLA functions, the basic idea is to shift the wing lift inboard by deflecting the outboard control surfaces (ailerons and spoilers) upward and sometimes also inboard control

surfaces (high speed ailerons and flaps) downward. For civil airliners, maneuvers are usually performed at relatively low frequencies and, if properly handled, interaction between maneuver load alleviation functions and flexible modes can largely be avoided. It is, for instance, common to cut (filter out) the pilot commands below the frequency of the first flexible modes of the airplane for comfort reasons and for preventing biodynamic coupling. The prevention of such interaction is not directly considered in this work, but could be included in future work. The evaluations made at the end of the paper consider dynamic pull-up/ push down maneuvers and not only the quasi-static pull-up/ push down maneuvers specified in [1, §331 b)].

3 CONSIDERED AIRCRAFT MODEL

3.1 Aircraft Configuration

The aircraft considered in this work is the SE^{2}A Mid-Range (MR) Aircraft [20]. Its top-level aircraft design requirements are similar to an Airbus A320-200. The mission profile of the SE²A MR is optimized to balance direct operating costs and CO_2-equivalent emissions [6]. In order to reduce contrail-emissions, the nominal mission profile is lower and slower than that of an A320-200. This mission profile led to a lower wing sweep angle. Additionally, both the wingspan and the aspect ratio are larger in comparison, while the wing loading is lower. One of the unconventional design features of this aircraft is the use of over-wing turbofan engines, with the engine inlet very close to the upper surface of the wing and a very aft position of the engine, see Figure 1. The aerodynamic benefits of such engine arrangements are being investigated by other groups in the SE^{2}A cluster. This feature has some impact on the aeroelastic behavior of the aircraft, but has fairly little impact on the work presented in this paper as the following baseline and MLA controller are mostly active at frequencies below the first flexible modes of the aircraft.

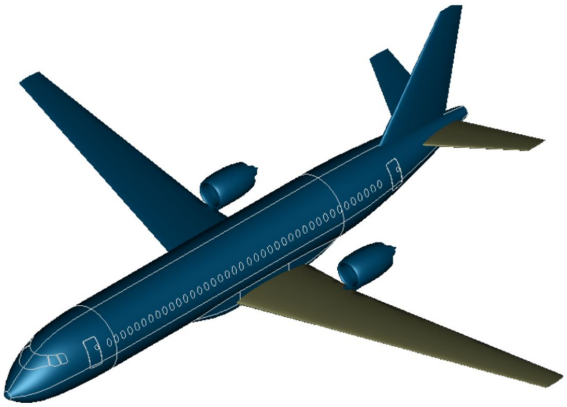

Figure 1: SE²A Mid-Range Aircraft, from [21]

The wing structure of the SE²A MR is sized to maneuver loads only. Gust loads are neglected in the structural sizing of the wing based on the assumption that a gust load alleviation system, e.g., the one from [6], reduces the gust loads down to the maneuver loads. The structural sizing was performed twice: first with the load envelope corresponding to a 2.5 g pull-up maneuver and then also for 2.0 g. The latter case yields an operational empty mass difference of two percent [21]. This indicates the mass reduction potential that can be obtained using a maneuver load reduction function, which ensure that the closed loop load envelope remains within the open loop load envelope obtained for a 2.0 g pull-up maneuver.

3.2 Nonlinear Model

The nonlinear aeroelastic flight dynamics model (FDM) documented in [21] is utilized for simulation of the given energy-efficient passenger airplane. The flexible structural model is based on a high-order finite-element model. Cut loads are computed at 134 load stations throughout the structure using the mode displacement method. The aerodynamics are implemented via a mid-fidelity unsteady model consisting of an unsteady airfoil model, dynamic stall model, and spanwise downwash model. The coupling of aerodynamics and structural dynamics is realized by handing the aerodynamic forces over to the flexible-body equations of motion [22] and feeding the resulting structure geometry back to the aerodynamic model. Actuators are modeled as second order systems with nonlinear constraints on both deflection and deflection rate (40 deg/s and 20 deg for the elevator). The simulation framework is capable of trimmming, linearizing, and simulating the aircraft throughout the flight envelope.

Due to the low torsional stiffness of the wings, the outboard ailerons have very little control authority at high dynamic pressures. Instead, micro-tabs presented in [23] are used in this work as Load Alleviation Devices (LAD) on the wing. They work similarly to spoilers, i.e., their deflection reduces lift locally through flow separation. Unlike conventional spoilers, micro-tabs do not rotate relative to the wing surface. Instead, they move perpendicular to it, and their deflection is expressed as a percentage of the local chord length $\%c$. Their maximum deflection is 2 $\%c$, and their spanwise location is identical to the outboard ailerons in [6], i.e., they reach from 81.7 % to 95.3 % of the wing half span. They are positioned at 60 $\%c$ in chord direction, providing good control authority on the local lift and low impact on the local pitching moment of the wing (and so indirectly on wing torsion). As for spoilers, micro-tabs can only decrease the local lift, so they are not applicable for maneuver load alleviation during push-down maneuvers.

At this stage of the work, only a steady aerodynamic model of the micro-tabs is considered, with a similar deflection rate limit to that of classical spoilers. This limit is imposed to ensure that the effectiveness and responsiveness of the micro-tabs is not over-estimated. For spoilers, the dimensionless deflection speed t_d^* is defined as:

$$t_d^* = t_d \frac{v_\infty}{c} \tag{1}$$

where t_d denotes the deflection time, v_∞ the undisturbed onflow velocity, and c the local chord length. Rapid deflection of spoilers leads to an instantaneous lift increase, followed by the intended lift reduction [24]. This phenomenon is also known as the spoiler adverse lift effect and does not occur for $t_d^* > 5...8$ (see [24,25]). The limitation regarding the micro-tab deflection rate derived from the spoiler adverse lift effect is introduced in section 4.2 and is assumed to be more restrictive than the mechanical deflection rate limit of the micro-tabs actuator.

3.3 Linear Model Processing

The coupled flight dynamics/aeroelastic nonlinear aircraft model can be trimmed and linearized around the considered flight conditions. This enables the application of a whole range of tools from linear control theory. For the example examined in the present paper, the point at the cruise speed boundary (cf. [21]) corresponding to the largest true airspeed is considered. In the present case, this corresponds to an altitude of 6000 m, an equivalent airspeed (EAS) of 177 m/s, a true airspeed (TAS) of 241 m/s and a Mach number of 0.76. The controller design is conducted with the linearized model at the aforementioned flight point with maximum take off

weight (MTOW). A series of additional linear models are generated similarly with longitudinal variations in center of gravity (CG) position throughout the flight envelope and will be used to evaluate the robustness of the proposed controllers.

Only the longitudinal dynamics are considered: the lateral dynamics are truncated based on the assumption that they are decoupled from the longitudinal dynamics. This assumption holds for wing-level steady state flight with negligible roll and sideslip angle and rate [26, 27]. The full-order linear models resulting from the trimming and linearization process have 800 states. A balanced truncation is performed based on Hankel singular values. Prior to the computation of the Hankel singular values, the model outputs are equalized based on the steady-state response to the considered inputs. Some outputs (e.g., wing root bending moment $M_{x,WR}$ in Nm) are several orders of magnitude larger than the others (e.g. Θ in deg, q in deg/s, or n_z in g) and would otherwise dominate the transfer function, which would then yield a very unbalanced reduced-order model quality (good match of the largest outputs, but poor match of the others). The resulting state-space models of the aircraft:

$$\mathbf{G_{AC}}: \begin{matrix} \dot{\mathbf{x}} = \mathbf{Ax} + \mathbf{Bu} \\ \mathbf{y} = \mathbf{Cx} + \mathbf{Du} \end{matrix} \tag{2}$$

has a state vector $\mathbf{x}$ with 75 states. The inputs $\mathbf{u} = [\delta_{E,cmd}, \delta_{LAD,cmd}]^T$ are the commanded elevator deflection and commanded load alleviation device deflection. All control surfaces are deflected symmetrically. The outputs $\mathbf{y} = [n_{z,CG}, q, V_{xz}, \Theta, M_{x,WR}, \delta_E, \dot{\delta}_E, \delta_{LAD}, \dot{\delta}_{LAD}]^T$ are the vertical load factor at the center of gravity, pitch rate, combined longitudinal and vertical inertial velocity in body-fixed frame (true airspeed), pitch angle, wing root bending moment, elevator deflection, elevator deflection rate, LAD deflection and LAD deflection rate. The outputs $n_{z,CG}$, q and Θ relate to rigid aircraft movement at the center of gravity. The linear models are converted to discrete time (using a zero-order hold method) to better represent a realistic flight control system with a sampling time T_s of 25 ms. Delays such as sensor delays, computational delays and transmission delays are assumed to sum up to 100 ms. They are applied as input delays at both plant inputs.

4 CONTROL DESIGN

This section presents the baseline control law and the maneuver load alleviation controller as well as their tuning. These control functions are tuned with a structured H_2/H_∞ method at a single design point and are scheduled over the dynamic pressure. Results for individual and combined controllers as well as further insight into the control design are presented in Section 5.

4.1 Design of the Baseline Control Law

As already understood for decades and used by Airbus since the A320 generation [13], letting pilots control the flight path angle γ or rather adjusting it by means of a load factor command (Δn_z is proportional to $\dot{\gamma}$) reduces their workload considerably. Indeed, pilots are less focused on stabilizing the flight path and correcting it in the presence of disturbances, as the control law handles this for them. Instead, they act as an outside-loop guidance law, i.e., they decide the required flight path. This fundamentally changes the role of the pilots, relieving them of low-level control tasks.

At high speed, limited angle of attack variations (and thereby also pitch rate) are sufficient to cause large variations of the load factor. However, at low speed, the range of load factor

variations is more limited and pilots were found to rather rely on the pitch rate [28, 29]. This observation led to considering a mix of the load factor at the pilot station $\Delta n_{z,pilot}$ and the pitch rate q for specifying the desired response to pilot stick inputs. This mixed signal is called C^* (C-star) and is defined as:

$$\Delta C^* = \Delta n_{z,pilot} + \frac{U_{co}\, q}{g} = \Delta n_{z,CG} + \frac{l_{pilot}\, \dot{q}}{g} + \frac{U_{co}\, q}{g} \tag{3}$$

where the crossover velocity $U_{co} = 122\, m/s$ defines the velocity above which C^* is dominated (in steady-state) by the $\Delta n_{z,pilot}$ term [28]. The load factor at the pilot station $\Delta n_{z,pilot}$ is affected by the center of gravity load factor $\Delta n_{z,CG}$, pitch acceleration $\dot{q}$, and distance from CG to cockpit l_{pilot} (for a rigid aircraft). Upper and lower bounds on the step response of C^* are a successor to the short-period-based longitudinal handling qualities requirements [29]. This is motivated by the fact that time envelopes of C^* not only contain information on the short-term dynamics and the effects on the pilot (normal acceleration, attitude changes, velocities and further accelerations), but also on actuator dynamics, higher order effects, and non-linear effects. Therefore, the baseline tracking performance will be evaluated with respect to the ΔC^* step response boundaries. The output vector **y** of the linear models is extended by the ΔC^* signal.

Figure 2 shows the baseline controller structure, which is based on [13, 14, 19]. The controller is implemented in discrete time and tracks the reference load factor commanded by the pilot $\Delta n_{z,CG}^{ref}$. The feedback path is primarily used for model error correction and disturbance rejection and consists of an integral load factor tracking feedback controller with the tunable parameter $K^I_{n_{z,CG}}$ as well as proportional pitch rate and load factor feedback with the tunable parameters K_q^P and $K^P_{n_{z,CG}}$. The dynamic feedforward controller $FF_{tf,tune}(z)$ is used to accelerate and shape the closed loop response to pilot inputs and is defined as a third-order transfer function with three tunable poles and three tunable zeros (defined using a `tunabletf` object in MATLAB).

Note that the tracking error output $n^e_{z,CG}$ and `analysis point` X_1 are only used during the tuning process. Analysis points are a priori defined points in the block diagram where the loop can be opened to extract one signal and inject another. X_1 is positioned at the plant input as this allows access to the input sensitivity function, which is used for the disturbance rejection and feedback stability margin requirements.

To compensate the dependence of the elevator effectiveness on the dynamic pressure, the elevator deflection is scheduled over the dynamic pressure q_{dyn} by scaling the baseline controller output with the ratio of design point dynamic pressure and current dynamic pressure $K_V = q_{dyn,DesignPoint}/q_{dyn}$. The rationale for choosing this particular gain scheduling can be explained as follows. Considering the aircraft trimmed at a given angle of attack α_{trim} with an elevator deflection $\delta_{E,trim}$ (a trimmable horizontal stabilizer is used here such that $\delta_{E,trim} = 0$). Applying a constant deflection $\delta_E = \delta_{E,trim} + \Delta\delta_E$ on the elevator yields a steady state angle of attack deviation[2] of $\Delta\alpha = \alpha - \alpha_{trim} = (C_{m,\delta_E} \,/\, C_{m,alpha})\, \Delta\delta_E$. This result usually holds for subsonic flight conditions and is generally acceptable in transonic conditions. The relationship between vertical load factor and angle of attack depends linearly on the dynamic pressure

[2] change of velocity of the aircraft neglected

(vertical force balance). For this reason, the relationship between elevator deflection and load factor is scaled with the dynamic pressure.

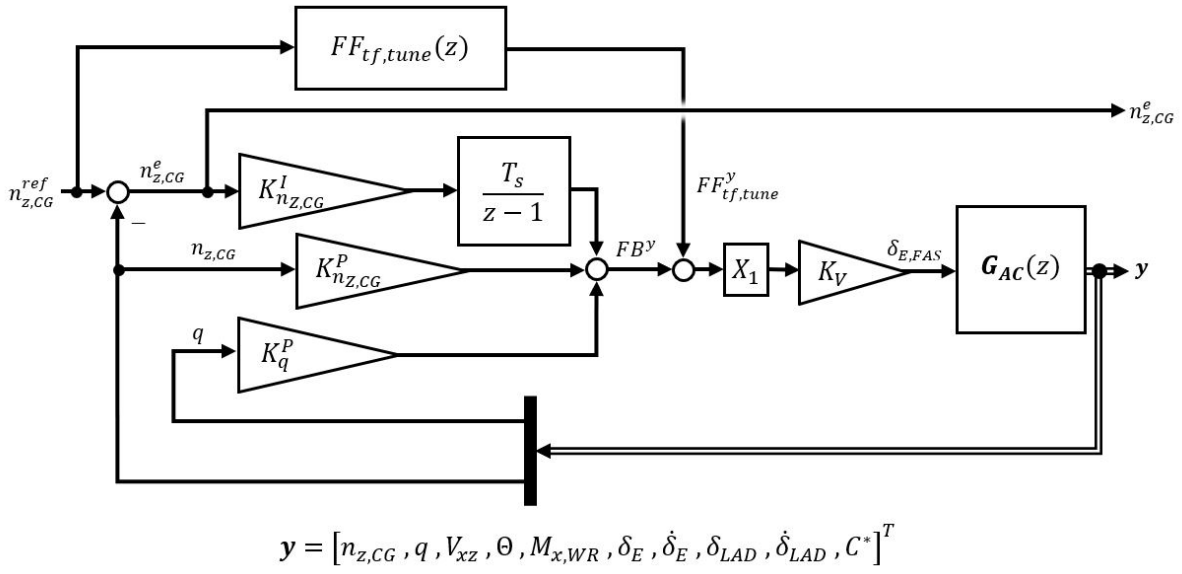

Figure 2: Baseline controller structure

The MATLAB `systune` framework [30] is utilized for the automated tuning process of both baseline and MLA controller. It allows for structured H_2/H_∞ control law synthesis, i.e., a control structure with fixed-order control elements can be defined a priori. The synthesis is based on non-smooth optimization techniques [31]. Tuning requirements can be defined either as 'hard' or 'soft' in the `systune` framework. Soft requirements are minimized, subject to hard requirements being met. The structured control synthesis is efficient and effective at handling large order systems (recall 75 states for the design system), but the lower order controller corresponds to a local optimum. It is therefore common practice to repeat the control synthesis with random start values to try to achieve a more favorable optimum. The tuning requirements are defined using H_2/H_∞ norms. These norms are applied here only to single-input single-output (SISO) systems, i.e., to transfer functions. The H_∞ norm of a transfer function is its largest gain for a sinusoidal input across all frequencies. An H_∞ requirement is formulated by multiplying the transfer function with a frequency-dependent weighting function and constraining the H_∞ norm of the augmented transfer function to an upper bound. The requirement is met if its performance η_R, i.e., the norm of the augmented transfer function, is smaller than one. The inverse of the weighting function, also known as a template, is denoted as $W^{-1}(s)$ and is used as an upper bound on the un-augmented transfer function. The same logic applies to H_2 requirements for SISO systems, however this norm is interpreted[3] as the energy of the output in response to an impulse [32]. The H_2 norm is employed in this work to reduce a system response across all frequencies. There are six hard tuning requirements for the baseline control law, which are summarized in Table 1 and explained below.

[3] other interpretations are available in [32]

Table 1: **Baseline controller tuning goals**

Goal	Description	Type	Location	Target
Hard Requirements				
1)	$n_{z,CG}^{ref}$ Tracking	H_∞	$T_{n_{z,CG}^{ref} \to n_{z,CG}^{e}}$	$\leq W_{e,n_{z,CG}}^{-1}(z)$ (Adjusted during tuning)
2)	$n_{z,CG}$ Tracking Overshoot	H_∞	$T_{n_{z,CG}^{ref} \to n_{z,CG}}$	$\leq 30\%$
3)	Feedback stability margin	`Margin`	X_1	$\geq [6\,dB, 45°]$
4)	Disturbance Rejection	`Rejection`	X_1	$\leq W_{reject}^{-1}(z)$
5)	Feedforward Controller Poles	`ControllerPoles`	$FF_{tf,tune}(z)$	$\omega_d < 100\,rad/s$ $\xi_d = 1$
6)	Elevator deflection rate	H_∞	$T_{n_{z,CG}^{ref} \to \dot{\delta}_E}$	$\leq \frac{40°/s}{1.5\,g}$

4.1.1 Reference Load Factor Tracking

For reference tracking, the closed loop transfer function $T_{ref \to e}$, where ref is the reference input and e is the tracking error, must decrease at low frequencies. To accelerate the system response, an overshoot of the tracking signal is usually allowed. For good noise suppression, the closed loop system should show little response to the tracking error at large frequencies. These demands are achieved by shaping $T_{ref \to e}$ with an H_∞ requirement. The tracking template is defined as a band-pass filter:

$$W_e^{-1}(s) = \frac{e_{Peak}s + \omega_{hpf}e_{DC}}{s + \omega_{hpf}} \cdot \frac{e_\Omega / e_{Peak}s + \omega_{lpf}}{1 + \omega_{lpf}} \tag{4}$$

with low frequency error e_{DC}, peak error e_{Peak}, high frequency error e_Ω, high-pass filter cut-off frequency $\omega_{hpf} = 2/t_{resp}$, response time t_{resp}, low-pass filter cutoff frequency $\omega_{lpf} = 2/(t_{resp}(1 - 1/\kappa_{reso}))$, and the width of the resonance window in which an increased tracking error is allowed κ_{reso}. Figure 3 visualizes the tracking template definition as both Frequency Response Data (FRD) and Transfer Function (TF). The FRD definition is included for visualization purposes only and is equivalent to the TF definition in the context of the `systune` framework (requirements can be defined using FRD but are converted to a TF). The reference tracking template for the baseline controller $W_{e,n_{z,CG}}^{-1}(z)$ is defined by Eq. (4), with $e_{DC} = 10^{-6}$ and $e_\Omega = 1.01$. Choosing $e_{Peak} = 3$ and $\kappa_{reso} = 2.2$ leads to an allowed tracking error of $6\,dB$ at the closed loop resonance frequency.

It is not straightforward to select the response time for a closed loop system constrained by a set of H_2/H_∞ requirements. Thus, an iterative approach is adopted: a tunable control structure along with its requirements is passed to `systune`. If the control synthesis fails to converge to a controller that satisfies all hard requirements ($\max\{\eta_R^{hard}\} > 1$), the tracking requirement

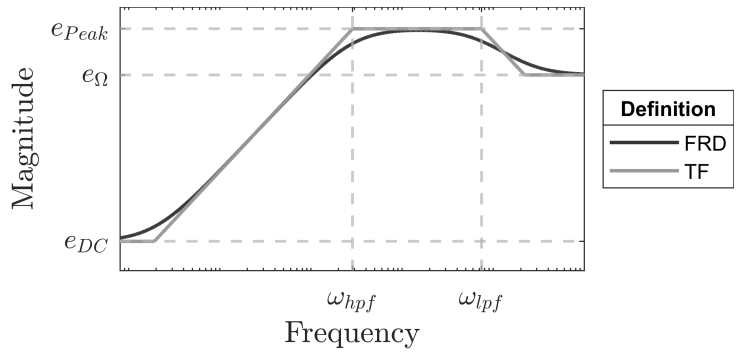

Figure 3: Tracking Template $W_e^{-1}(s)$

is relaxed by increasing the response time. If no satisfactory controller is obtained after n_{rand} random restarts, the tracking requirement is iteratively relaxed until a satisfactory solution is reached, see Algorithm 1. The permissible response time $t_{resp,max}$ is defined a priori to limit the number of iterations. The initial required response time is chosen low enough that Algorithm 1 fails on its first iteration to ensure that the quickest closed loop response satisfying all requirements is achieved. Regarding the baseline controller, the load factor tracking template $W_{e,n_{z,CG}}^{-1}(z)$ is initiated with a response time of $400\,ms$. Further requirements are presented below.

Algorithm 1 Control synthesis with iterative tracking performance relaxation

while $\max\{\eta_R^{hard}\} > 1 \quad \&\& \quad t_{resp} < t_{resp,max}$ **do**
  Increase response time t_{resp} by $5\,\%$
  Update tracking template $W_e^{-1}(s)$
  Synthesize a controller using `systune` with n_{rand} random restarts
end while

4.1.2 Load Factor Tracking Overshoot

The overshoot of the tracking signal is constrained to $30\,\%$ to ensure that the C^* step response bounds are met. This is applied via an H_∞ constraint on the transfer function from reference load factor input ($n_{z,CG}^{ref}$) to load factor output ($n_{z,CG}$). Note, that the H_∞ norm of the transfer function is used as an overshoot estimate based on the analogy to second-order model characteristics.

4.1.3 Stability margins

A stability margin requirement is applied to provide robustness against system uncertainties. Classical gain and phase margins $GM|PM$ of at least $6\,dB|45°$ are specified as unskewed disk margins at the analysis point X_1 in Figure 2. They are realized using the `Margin` requirement. Its performance is defined as $\eta_{R,Margin} = ||2\alpha S - \alpha I||_\infty$, where S is the sensitivity function and α denotes a parameter based on the specified gain margin and phase margin $\alpha = 2 \cdot \max\{(GM-1)/(GM+1), tan(PM/2)\}$ [30].

4.1.4 Disturbance and Model Error Rejection

The reference tracking may largely be achieved via the feedforward filter $FF_{tf,tune}(z)$. However, the real-world system differs from the model considered during tuning. To ensure that the remaining model error is compensated in a timely manner, some minimum level of rejection must be provided by the feedback controller. Using the loop transfer function at point X_1

(cf. Figure 2) allows the effect of input disturbances and multiplicative input uncertainty to be specified. The transfer function from input disturbance to the signal prior to its injection has a gain of $0\,dB$ at high frequencies as the feedback controller cannot compensate perturbations at high frequencies. By specifying an H_∞ template $W_{reject}^{-1}(z)$ that is sufficiently small at low frequencies, a minimum disturbance / model error rejection can be ensured, which is achieved through the integral feedback controller. At high frequencies, the template is raised above $0\,dB$ to provide the synthesis with enough design freedom to find a feedforward filter that improves the immediate tracking response.

4.1.5 Feedforward Filter Poles

Achieving good reference tracking for the nominal system via the feedforward filter $FF_{tf,tune}(z)$ using an inverse controller:

$$FF_{tf,tune}(z) \approx \left(\mathbf{G_{AC}}(z)\right)^{-1} \; K_V^{-1} \tag{5}$$

may seem very attractive (provided no further restrictions and no feedback). This leads, however, to solutions lacking robustness. Even on the nominal system and if the nominal system did not have unstable zeros (which would lead to an unstable inversion feedforward controller), the plant inversion will achieve a quick response at the cost of large and often oscillatory control commands. To prevent such effects, the pole locations of the feedforward filter are constrained regarding frequency ($\omega_d \leq$100$\,rad/s$) and damping ($\xi_d =$1). This limits the feedforward bandwidth and eliminates oscillatory feedforward filter outputs, i.e., control commands.

4.1.6 Limit on Elevator Commands

It is highly advisable to tune the controller such that it complies with actuator deflection and deflection rate saturation limits. Reaching the saturation limits may result in degraded closed-loop performance or even loss of stability (in the case of feedback control). To prevent saturation of the elevator actuator deflection rate, the H_∞ norm of the transfer function from the reference input ($n_{z,CG}^{ref}$) to the actuator deflection rate output ($\dot{\delta}_E$) is constrained to the actuator deflection rate limit ($40°/s$) relative to the largest expected reference input ($\Delta n_{z,CG}^{ref} =$1.5$\,g$ for a 2.5$\,g$ pull-up maneuver). It is worth mentioning that this requirement does not generally restrict the controller from saturating the elevator actuator deflection rate. Rather, it ensures at the design point that $\dot{\delta}_E$ remains below $40°/s$ for sinusoidal reference inputs correlating with 2.5 g pull-up maneuvers at all frequencies. Like in [6], requirements are specified for the deflection rate only, since the deflections themselves rarely reach their limits at the considered flight conditions.

4.2 Design of the Maneuver Load Alleviation Function

The MLA function is designed to reduce the wing root bending moment during maneuvers. As a result, the sizing loads resulting from the requirements for the symmetrical maneuvering conditions in accordance with [1, §331] are also reduced. The set of symmetrical maneuver conditions (balanced, maximum pitch controller displacement, and checked maneuvers) are to be conducted with the maximum positive and negative load factors (defined by [1, §337]). Only the maximum positive load factor is considered here for two reasons: Firstly, the design loads include the trim loads, so that upward bending moments, for example, are typically critical. Secondly, the selected LAD can only reduce lift, thus the maneuver load alleviation is only applicable for positive load factors. The maximum positive load factor is +2.5$\,g$ [1] for the

given aircraft at speeds above the intersection of the stall boundary and maximum positive load factor. Below this intersection speed, the maneuver loads are irrelevant for the structural sizing.

The MLA function aims at mitigating the inboard bending moment by shifting the lift distribution towards the plane of symmetry of the aircraft. To achieve this, the MLA function consists of a nonlinear activation logic and a linear lift redistribution controller, see Figure 4. The activation logic $\boldsymbol{MLA_{trigger}}$ feeds a reference LAD deflection $\delta^{ref}_{LAD} = 2\,\%c$ (maximum LAD deflection) to the lift redistribution controller if $\Delta n_{z,CG}$ exceeds 0.5 g and deactivated if $\Delta n_{z,CG}$ stays for two seconds below 0.2 g. The waiting period is a safety feature to prevent coupling of the LAD deflection with buffeting effects or some flexible mode. The structural sizing maneuvers reliably activate the $\Delta n_{z,CG}$-trigger, though an alternative trigger may replace it in future projects to capture edge-case maneuvers [11].

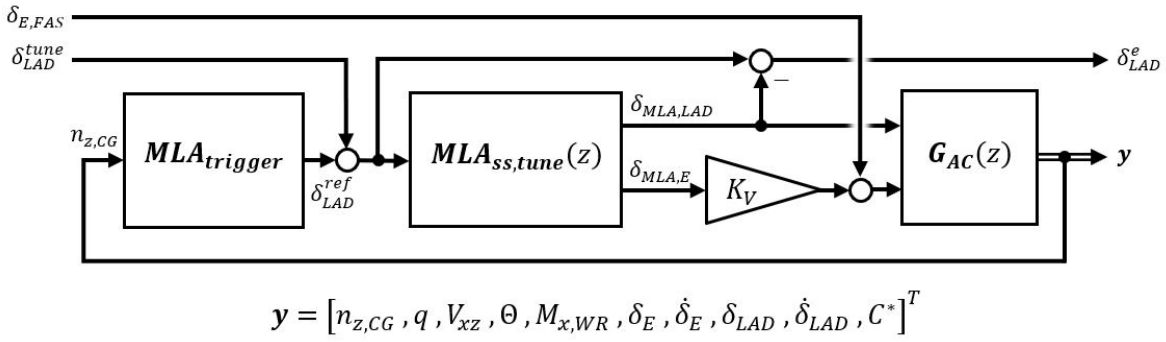

Figure 4: Maneuver load alleviation controller structure

Once the MLA is activated, the outboard lift is reduced by deflecting the outboard LAD. To avoid impairing the desired flight path, the lift reduction is compensated by increasing the angle of attack. The most simple version of the lift redistribution is to deflect the LAD and then utilize the baseline feedback controller to adjust the angle of attack by deflecting the elevator. However, the baseline controller reaction is relatively slow, causing a transitory flight path disturbance which impairs the ride comfort. It can be accelerated using a proportional cross-feed to the elevator based on the low frequency system dynamics of $\boldsymbol{G_{AC}}$. Nevertheless, since the LAD actuator is much quicker than the elevator actuator, the proposed proportional feedforward controller would abruptly decrease the outer lift while the inner lift increase lags behind, causing the wings structure to oscillate.

Hence, the lift redistribution commands are defined via a dynamic lift redistribution controller $\boldsymbol{MLA_{ss,tune}}(z)$. This feedforward controller is tuned utilizing the structure depicted in Figure 4. It is a tunable state-space model with one input δ^{ref}_{LAD}, two outputs $[\delta_{MLA,LAD}, \delta_{MLA,E}]^T$ and five states. Note that the difference of LAD command input and LAD reference deflection δ^{e}_{LAD} is only used during the tuning process. The elevator deflection is scheduled over the dynamic pressure through K_V (cf. Section 4.1). The MLA is combined with the baseline controller via the elevator command from the latter $\delta_{E,FAS}$. The input δ^{tune}_{LAD} is later utilized in section 5.1.2 to demonstrate the system response to the lift redistribution in horizontal flight for both proportional and dynamic feedforward controllers.

The automated tuning of the MLA lift redistribution controller is analogous to that of the baseline controller and is defined by seven requirements which are summarized in Table 2 and explained below.

Table 2: **Lift redistribution (MLA) controller tuning goals**

Goal	Description	Type	Location	Target
Hard Requirements				
1)	δ_{LAD}^{ref} Dynamics	H_∞	$T_{\delta_{LAD}^{ref} \to \delta_{LAD}^{e}}$	$\leq W_{e,\delta_{LAD}}^{-1}$ (Adjusted during tuning)
2)	δ_{LAD} Overshoot	H_∞	$T_{\delta_{LAD}^{ref} \to \delta_{LAD}}$	$\leq 10\%$
3)	Ride Comfort, Low Disruption of desired Flight Path	H_∞	$T_{\delta_{LAD}^{ref} \to n_{z,CG}}$	$\leq \frac{0.5\%g}{2\%c},\ \forall\, \omega < 10\, rad/s$
4)	LAD deflection rate	H_∞	$T_{\delta_{LAD}^{ref} \to \dot{\delta}_{LAD}}$	$\leq \frac{35.4\%c/s}{2\%c}$
5)	Elevator deflection rate	H_∞	$T_{\delta_{LAD}^{ref} \to \dot{\delta}_{E}}$	$\leq \frac{40°/s}{2\%c}$
Soft Requirements				
6)	Limit on Elevator Command	H_2	$T_{\delta_{LAD}^{ref} \to \dot{\delta}_{E}}$	$\leq 5\%$
7)	Low $M_{x,WR}$ Excitation	H_2	$T_{\delta_{LAD}^{ref} \to M_{x,WR}}$	$\leq 5\%$

4.2.1 LAD Reference Deflection Dynamics

The LAD is deflected according the output of the MLA activation logic by constraining the transfer function from reference (δ_{LAD}^{ref}) to the difference of command input and reference (δ_{LAD}^{e}) to the reference tracking template ($W_{e,\delta_{LAD}}^{-1}$). This effectively constrains the minimum bandwidth of the feedforward dynamics and shapes the dynamic of the LAD deflection. Analogous to the baseline controller, the demand on a quick response of the lift redistribution controller is iteratively relaxed using Algorithm 1 (page 10) until all other hard requirements can be met. The template is defined by Eq. (4) with $e_{Peak} = 2$, $\kappa_{reso} = 2.2$, e_{DC} =10^{-6}, e_{Ω} =1.1, and initially $t_{resp} = 300\, ms$.

4.2.2 LAD Deflection Overshoot

The overshoot of the LAD deflection is constrained to 10 % to restrict the velocity at which the LAD reaches its end-stop. Setting the overshoot constraint to zero would result in a unnecessarily slow LAD deflection. This requirement is applied via an H_∞ constraint on the transfer function from reference (δ_{LAD}^{ref}) to the LAD deflection output (δ_{LAD}). Note, that the H_∞ norm of the transfer function is used as an overshoot estimate based on the analogy to second-order model characteristics.

4.2.3 Ride Comfort, Low Disruption of Desired Flight Path

Once the $\boldsymbol{MLA_{trigger}}$ is active, it feeds a reference LAD deflection of $2\,\%c$ to the lift redistribution controller. During lift redistribution, the aircraft should remain on the desired flight path with little vertical acceleration disturbance to provide good ride comfort and minimal baseline controller disturbance. This is ensured by limiting the output $\Delta n_{z,CG}$ to $0.005\,g$ at low frequency for the largest expected reference input ($\delta^{ref}_{LAD} = 2\,\%c$) using a frequency-limited H_∞ requirement.

4.2.4 Limit on LAD Commands

Rapid deflection of the LAD is expected to cause the non-linear adverse lift effect (cf. Section 3). Hence, the LAD deflection rate is constrained to $t^*_d = 10$. This deflection time is equivalent to a peak LAD deflection rate of $35.4\,\%c/s$ at the design flight point (cf. eq. 1). An H_∞ requirement is used to constrain the transfer function from reference (δ^{ref}_{LAD}) to LAD deflection rate ($\dot{\delta}_{LAD}$) to the ratio of LAD deflection rate limit ($35.4\,\%c/s$) and the largest expected reference input ($2\,\%c$).

4.2.5 Limit on Elevator Commands

Saturation of the elevator actuator deflection rate is prevented by constraining the H_∞ norm of the transfer function from the reference (δ^{ref}_{LAD}) to the elevator deflection rate ($\dot{\delta}_E$) to ratio of elevator actuator deflection rate limit ($40°/s$) and the largest expected reference input ($2\,\%c$).

4.2.6 Elevator Control Effort and Structural Oscillation

The soft requirements are defined so that they prevent unnecessarily high elevator deflection rates (H_2 requirement on elevator deflection rate) and minimize the excitation of structural modes caused by the LAD deflection (H_2 requirement on wing root bending moment). The target values of the soft requirements are $5\,\%$ of the respective low-frequency magnitude, so that they are weighted equally in the synthesis. Since the other requirements force the LADs to be deflected, only higher-frequency system responses are affected by these requirements.

5 RESULTS

5.1 Performance of Individual Controllers

Algorithm 1 (page 10) is utilized to synthesize both controllers. To provide insight into the control design, their performance is tested individually in this section: the FAS is tested with the MLA suppressed, and vice versa.

5.1.1 Nominal Performance of Baseline Controller

The baseline controller with both feedforward and feedback paths (FBFF) is compared to one tuned without the feedforward path (FB). The tracking performance for a 2.5 g pull-up maneuver is shown in Figure 5. The feedforward controller initially outputs a large signal, such that the elevator is quickly deflected, accelerating the system response. As a result, the FBFF controller meets the ΔC^* step response limits despite the large input delay. Without the feedforward controller the response is significantly slower, such that the step response boundaries are violated. The elevator deflection is far below the saturation limit of 20°. Since the elevator deflection rate constraint (see section 4.1.6) is applied to all frequencies up to the Nyquist frequency, the peak deflection rate is well below the saturation limit of $40°/s$.

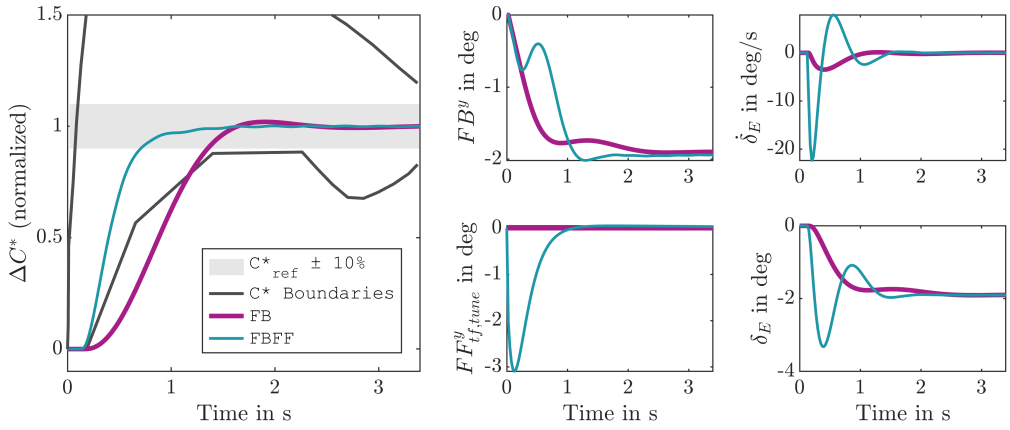

Figure 5: Step response with baseline controller, critical flight point, linear reduced system

5.1.2 Nominal Performance of MLA Lift Redistribution

This section compares different design approaches for the MLA lift redistribution controller. As previously mentioned, the outboard lift decrease is compensated by an increase in the angle of attack. The elevator deflection is used to compensate the pitching moment of the deflected LAD and is applied using a cross-feed. This can be designed either statically (proportional feedforward) or dynamically. Both approaches are compared here.

The MLA lift redistribution controller is tested without FAS in horizontal flight. For this demonstration, $\delta_{E,FAS}$ is set to zero and a step signal is fed to δ_{LAD}^{tune}, cf. Figure 4. Using a dynamic lift redistribution controller instead of a static one provides better ride comfort regarding the vertical acceleration and reduces the structural oscillation, see Figure 6. The LAD deflection reduces the outboard lift and also produces a pitch-up moment. A pitch-down elevator command (trailing edge down) is used to alleviate the pitch-up movement induced by the LAD deflection. In the end, the lift redistribution exerts minimal influence on the load factor and pitch rate. Consequently, the MLA activation is expected to have minimal influence on the FAS, such that the

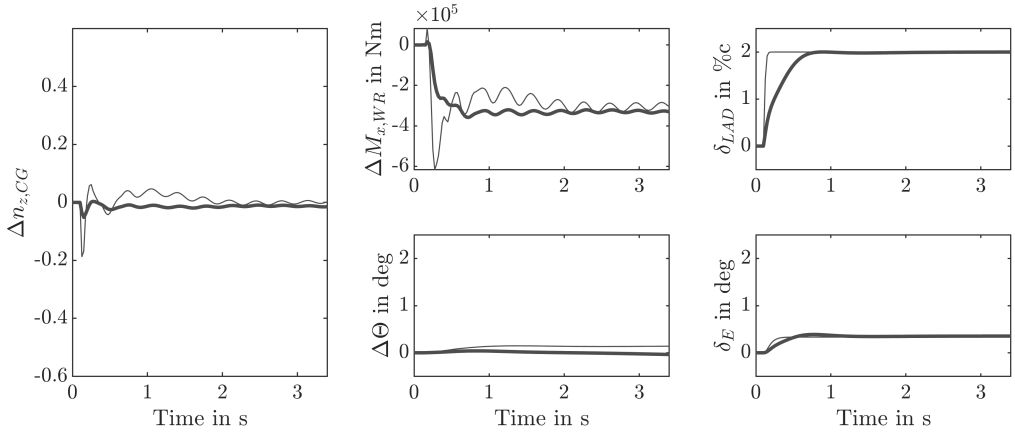

Figure 6: Step response of static (——) and dynamic (▬) lift redistribution in horizontal flight, critical flight point

baseline controller is largely decoupled from the MLA and pilots can be expected to hardly notice the activation of the MLA function.

5.2 Performance of Combined Controllers

5.2.1 Nominal Performance

The combined baseline controller and MLA function are evaluated in this section. Figure 7 compares the system response for a 2.5 g doublet maneuver at the critical flight point with and without MLA. Once $\Delta n_{z,CG}$ exceeds 0.5 g the LADs are deflected, decreasing the wing root bending moment. A relative load reduction regarding the wing root bending moment:

$$\Delta LA = (\max_t(\Delta M_{x,WR}^{withMLA}(t)) - \max_t(\Delta M_{x,WR}^{withoutMLA}(t))) \,/\, \max_t(\Delta M_{x,WR}^{withoutMLA}(t)) \quad (6)$$

of 9.1 % is achieved through the maneuver load alleviation. Moreover, the elevator deflection is altered through the cross-feed term of $\boldsymbol{MLA_{ss,tune}}(z)$ such that the pitch angle and load factor show very little difference compared to the response without MLA.

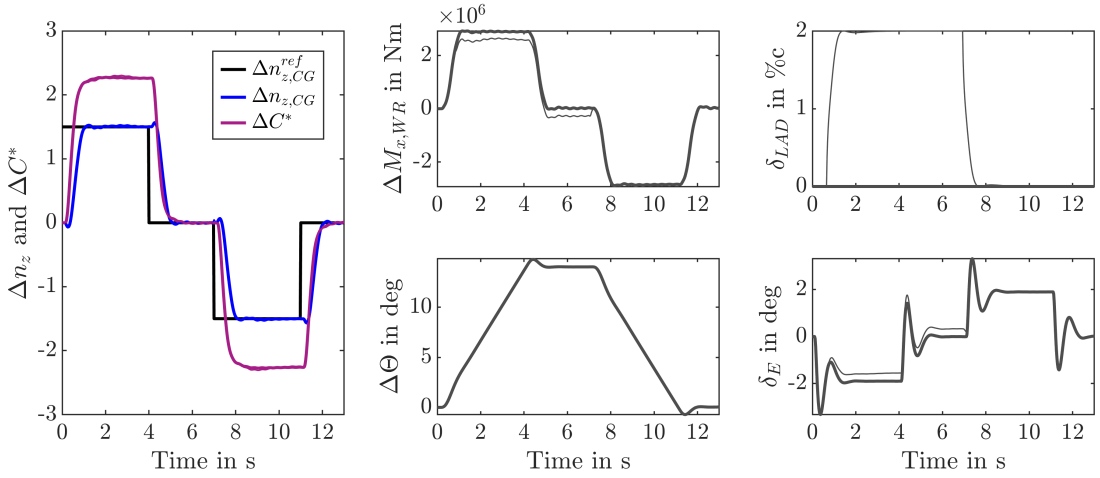

Figure 7: 2.5 g doublet maneuver at critical flight point with MLA (——) and without MLA (▬)

5.2.2 Robustness Cases

At last, the combined baseline controller and maneuver load alleviation are evaluated regarding their robustness against practical system variations, i.e., regarding simultaneous altitude variations (from 4 km up to 8 km), velocity variations (dive velocity V_D, cruise velocity V_C, and intermediate velocity in between maneuver velocity V_A and cruise velocity $(V_A + V_C)/2$), as well as center of gravity variations (as percentage of the Mean Aerodynamic Chord (MAC)). The maneuver visualized in Figure 7 is conducted for the robust cases with and without MLA. Performing the simulation with the fully linear systems $\mathbf{G_{AC}}$ causes the elevator actuator to exceed its deflection rate saturation limit for some operating points. To provide a more accurate system performance investigation, nonlinear actuator dynamics including saturation limits for both deflection and deflection rate are considered hereafter.

Figure 8 shows the resulting system responses. The combined controllers show good robust performance with respect to the applied variations, meeting the ΔC^* step response boundaries throughout (except for some low altitude and low velocity cases). The relative load alleviation reaches from 7.7 % up to 10.9 %. Deflecting more LAD sections in spanwise direction (see definition of LAD position in section 3.2) or extending the LAD further would allow increasing the load alleviation at the expense of additional drag and in-plane wing bending. The largest relative load reduction is observed at the operating point with rear-shifted CG at 4 km altitude and intermediate velocity. The tracking performance at this point is inadequate, as the ΔC^* step response boundaries are violated. This could be improved by re-tuning the controller gains throughout the flight envelope (controller gain scheduling). At 8 km altitude, intermediate velocity and default center of gravity position, the closed loop satisfies the ΔC^* step response boundaries despite the fact that the elevator actuator deflection rate reaches its saturation limit. The prolonged tracking overshoot for the latter two flight points is expected to be eliminated by the proposed controller gain scheduling as well.

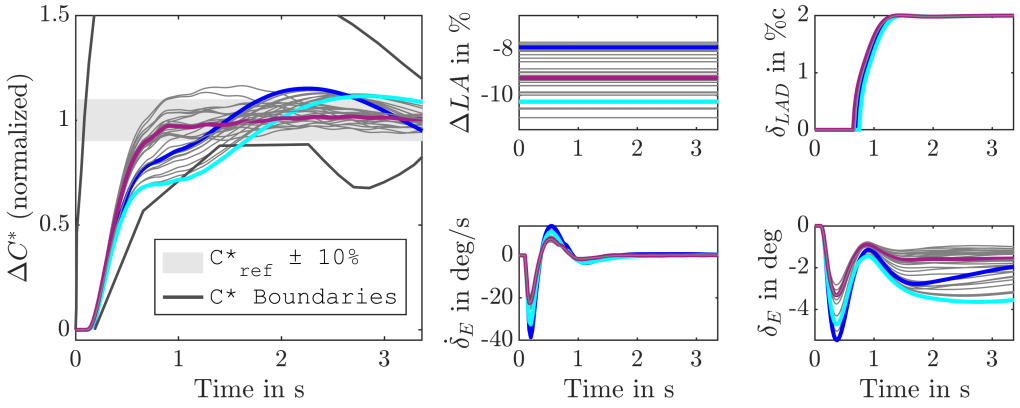

Line	CG-Offset	Altitude	Velocity
	[+2,0,-2] %MAC	[4,5,6,7,8] km	[(V$_C$+V$_A$)/2, V$_C$, V$_D$]
	0	6 km	V$_C$
	+2 %MAC	4 km	(V$_C$+V$_A$)/2
	0	8 km	(V$_C$+V$_A$)/2

Figure 8: Closed loop performance for 2.5 g pull-up maneuvers throughout the flight envelope with combined controllers (simulated using linear systems with nonlinear actuator saturation limits regarding both deflection and deflection rate)

6 SUMMARY AND OUTLOOK

Two automated controller design approaches were presented for the synthesis of a baseline load factor / C^*-based control law and of a maneuver load alleviation function. The aim of these automated processes is twofold: first, to support (pre-)design studies through automatic adjustment of these controllers during the design loop and second, to potentially serve as starting point for fine tuning of such functions by a control specialist. Overall, the control design problems and tasks remain challenging, such that a certain expertise with modern control design tools is required to apply the proposed approach.

The considered load alleviation devices are micro-tabs and, like spoilers, work by reducing the local lift through flow separation on the upper-surface of the wing. They are located at an outboard position, upstream of the ailerons. The evaluations, performed with center of gravity variations and flight points in a portion of the envelope, showed a maneuver load alleviation performance of 7.7–10.9 %, considering each model and flight point separately (with MLA versus without in each case). This performance could certainly be increased by also using micro-tabs sections further inboard, i.e. where outboard spoilers are usually installed. The LAD commands are rather simple in shape, but activated and deactivated in a nonlinear way and with a time-based hysteresis to prevent any undesirable coupling with the structure and potential buffeting effects. The dynamics of the MLA controller are tuned so that unnecessary excitation of the wing modes and unnecessary trajectory disturbance are avoided during (de)activation. The natural pitch-up tendency of the aircraft upon deflection of the micro-tabs is automatically alleviated by a pitch-down elevator command. As a result, the aircraft only pitches up during MLA activation to compensate for the reduced outboard lift, maintaining the same load factor as it would have been without MLA activation.

The controllers are scheduled based on dynamic pressure and perform well across the considered flight points of loading cases. No scheduling with CG position was made, which explains the slight change in behavior with CG position. This variation remains reasonable and would probably remain hardly noticed by most pilots. There are certainly numerous ways to improve the proposed controllers and control design methodology. The value of the time delay before retracting the micro-tabs as well as the dynamics of this retraction have not been investigated in details. The need and possible ways to perform MLA in the opposite direction, i.e., push-down maneuvers, should also be assessed. Improvements of the robustness to flight point and CG variations could probably be obtained by integrating a reference response model in the command path of the integral feedback controller, as this would allow increasing its gain without increasing the load factor tracking overshoot.

ACKNOWLEDGMENTS

We would like to acknowledge the funding by the Deutsche Forschungsgemeinschaft (DFG, German Research Foundation) under Germany´s Excellence Strategy – EXC 2163/1 - Sustainable and Energy Efficient Aviation – Project-ID 390881007.

7 REFERENCES

[1] EASA (2023). *CS-25: Certification specifications and acceptable means of compliance for large aeroplanes*. Amendment 27, European Union Aviation Safety Agency.

[2] Allison, R. L., Perkin, B. R., and Schoenmann, R. L. (1978). Application of winglets and/or wing tip extensions with active load control on the Boeing 747. Tech. Rep.

19780021107, NASA. Langley Research Center CTOL Transport Technologies. https://ntrs.nasa.gov/citations/19780021107.

[3] White, R. J. (1971). Improving the airplane efficiency by use of wing maneuver load alleviation. *Journal of Aircraft*, 8(10), 769–775. DOI:10.2514/3.59169.

[4] Johnston, J. F. (1982). Accelerated development and flight evaluation of active controls concepts for subsonic transport aircraft. Tech. Rep. 19820007204, NASA Contractor Report.

[5] Wallace, C. and Fezans, N. (2023). Lidar-based gust load alleviation - results obtained on a generic long range aircraft configuration. In *CEAS – EUCASS Aerospace Europe Conference 2023*. DOI:10.13009/EUCASS2023-564.

[6] Cavaliere, D. and Fezans, N. (2024). A practical approach to automated multiobjective gust load alleviation control design in a structured H_2 / H_∞ framework. Bristol, UK. CEAS-GNC-2024-042.

[7] Fournier, H., Massioni, P., Tu Pham, M., et al. (2022). Robust gust load alleviation of flexible aircraft equipped with lidar. *Journal of Guidance, Control, and Dynamics*, 45(1), 58–72. DOI:10.2514/1.G006084.

[8] Bussemaker (2018). *Wing Optimization With Active Load Control*. Master's thesis, Technical University Delft and Airbus Aeromechanics Systems. http://resolver.tudelft.nl/uuid:099604d8-c056-471c-b003-e31605523074.

[9] Handojo, V. (2020). *Contribution to Load Alleviation in Aircraft Predesign and Its Influence on Structural Mass and Fatigue*. PhD Thesis, Technical University Berlin. Published as DLR Research Report DLR-FB-2020-47. ISSN: 1434-8454. ISRN: DLR-FB–2020-47.

[10] Wunderlich, T. F., Dähne, S., Reimer, L., et al. (2021). Global aerostructural design optimization of more flexible wings for commercial aircraft. *Journal of Aircraft*, 58(6), 1254–1271. DOI:10.2514/1.C036301.

[11] Pereira, M., Kolmanovsky, I., Cesnik, C., et al. (2019). Model predictive control for maneuver load alleviation in flexible airliners. In *IFASD 2019*. Savannah, GA, USA.

[12] Krengel, M. (2022). Basic maneuver load alleviation in conceptual aircraft design. In *22th ONERA-DLR Aerospace Symposium*. Hamburg, Germany. https://elib.dlr.de/186721/.

[13] Favre, C. (1994). Fly-by-wire for commercial aircraft: the airbus experience. *International Journal of Control*, 59(1), 139–157. DOI:10.1080/00207179408923072.

[14] Delannoy, S. and Oudin, S. (2013). Longitudinal control law for modern long range civil aircrafts. In *EuroGNC 2nd CEAS Specialist Conference on Guidance, Navigation & Control*. Delft, The Netherlands. https://aerospace-europe.eu/media/books/delft-0027.pdf.

[15] Harris, J. J. (2018). F-35 flight control law design, development and verification. In *2018 Aviation Technology, Integration, and Operations Conference*. DOI:10.2514/6.2018-3516.

[16] Puyou, G., Bérard, C., Ferreres, G., et al. (2006). Conception multi-objectif de lois de pilotage pour un avion de transport civil. *Journal Europeen des Systemes Automatises*, 40(1). DOI:10.3166/jesa.40.1019-1051.

[17] Guinn, W. A., Rising, J. J., and Davis, W. J. (1984). Development of an advanced pitch active control system for a wide body jet aircraft. Tech. Rep. 19870008280, NASA Contractor Report. https://ntrs.nasa.gov/citations/19870008280.

[18] Berger, T., Tischler, M., Hagerott, S. G., et al. (2017). Handling qualities flight test assessment of a business jet NzU p-beta fly-by-wire control system. In *2017 AIAA Atmospheric Flight Mechanics Conference / SciTech Forum*. Grapevine, TX, USA. DOI:10.2514/6.2017-1398.

[19] Pérez, C. A., Theodoulis, S., Sève, F., et al. (2022). Automatic weighting filter tuning for robust flight control law design. *IFAC 18th IFAC Workshop on Control Applications of Optimization*, 55(16), 400–405. ISSN 2405-8963. DOI:10.1016/j.ifacol.2022.09.057.

[20] Karpuk, S., Radespiel, R., and Elham, A. (2022). Assessment of future airframe and propulsion technologies on sustainability of next-generation mid-range aircraft. *Aerospace*, 9(5). ISSN 2226-4310. DOI:10.3390/aerospace9050279.

[21] Beyer, Y., Cavaliere, D., Bramsiepe, K., et al. (2023). An aeroelastic flight dynamics model for gust load alleviation of energy-efficient passenger airplanes. In *AIAA AVIATION 2023 Forum*. DOI:10.2514/6.2023-4452.

[22] Waszak, M. R. and Schmidt, D. K. (1988). Flight dynamics of aeroelastic vehicles. *Journal of Aircraft*, 25(6), 563–571. DOI:10.2514/3.45623.

[23] Khalil, K., Asaro, S., and Bauknecht, A. (2022). Active flow control devices for wing load alleviation. *Journal of Aircraft*, 59(2), 458–473. DOI:10.2514/1.C036426.

[24] Geisbauer, S. (2021). Numerical simulation and validation of aerodynamics of static and dynamic spoilers. *Journal of Aircraft*, 58(6), 1187–1203. DOI:10.2514/1.C036145.

[25] Maboy, D. (1983). Experimental methods to determine control effectiveness in wind tunnels. In *AGARD Special Course on Aerodynamic Characteristics of Controls*, vol. 711. ISBN: 978-92-835-1457-2.

[26] Stevens, B., Lewis, F., and Johnson, E. (2016). *Aircraft Control and Simulation*. New Jersey: Wiley & Sons, 3. ed. ISBN: 978-1-118-87098-3.

[27] Boiffier, J.-L. (2000). *The Dynamics of Flight: The Equations*. New York: Wiley & Sons. ISBN: 978-0-470-86052-6.

[28] Sutherland, J. P. (1968). *Fly-by-wire flight control systems*. Air Force Flight Dynamics Lab Wright-Patterson AFB OH. https://apps.dtic.mil/sti/citations/AD0679158.

[29] Field, E. (1993). *The Application of a C Flight Control Law to Large Civil Transport Aircraft*. College of Aeronautics report. College of Aeronautics, Cranfield Institute of Technology. ISBN: 978-1-871564-58-7.

[30] MathWorks (2023). Control system toolbox R2023b. Tech. rep., The MathWorks, Inc.

[31] Apkarian, P. and Noll, D. The H_∞ control problem is solved. *Aerospace Lab*, 13(1). DOI:10.12762/2017.AL13-01.

[32] Skogestad, S. and Postlethwaite, I. (2005). *Multivariable Feedback Control: Analysis and Design*. New York: Wiley & Sons, 2^{nd} ed. ISBN: 978-0-470-01167-6.

COPYRIGHT STATEMENT